PCCP

PAPER

Cite this: *Phys. Chem. Chem. Phys.*, 2015, **17**, 16398

A first-principles study of sodium adsorption and diffusion on phosphorene†

Xiao Liu,[a] Yanwei Wen,*[b] Zhengzheng Chen,[b] Bin Shan[bc] and Rong Chen*[a]

Received 26th April 2015,
Accepted 11th May 2015

DOI: 10.1039/c5cp02419f

www.rsc.org/pccp

The structural, electronic, electrochemical as well as diffusion properties of Na doped phosphorene have been investigated based on first-principles calculations. The strong binding energy between Na and phosphorene indicates that Na could be stabilized on the surface of phosphorene without clustering. By comparing the adsorption of Na atoms on one side and on both sides of phosphorene, it has been found that Na–Na exhibits strong repulsion at the Na–Na distance of less than 4.35 Å. The Na intercalation capacity is estimated to be 324 mA h g^{-1} and the calculated discharge curve indicates quite a low Na^+/Na voltage of phosphorene. Moreover, the diffusion energy barrier of Na atoms on the phosphorene surface at both low and high Na concentrations is as low as 40–63 meV, which implies the high mobility of Na during the charge/discharge process.

1. Introduction

Rechargeable solid-state batteries have entered our daily life and are being widely used in portable electronics, electrical vehicles, and miscellaneous power devices.[1–4] Due to the abundance of sodium (Na) and low redox potential (−2.71 V *vs.* standard hydrogen electrode),[5,6] sodium-ion batteries (SIBs) have attracted much attention to fulfill the urgent need for Li-ion batteries (LIBs), especially for large-scale energy storage. As a key component of SIBs, the anode materials are desired to possess high Na capacity, low redox potential, high electronic conductivity, high-rate Na diffusivity and robust structural stability.[7] Graphite, the commercial anode material for LIBs, is not very appropriate to encapsulate the Na effectively, due to the weak interaction between Na and the graphene plane, which affects the electrochemical perfermance.[8–10] Other carbon-based structures (hard carbon, porous carbon), as well as porous and layered oxide materials (TiO_2, $K_{0.8}Ti_{1.73}Li_{0.27}O_4$, $Na_2Ti_3O_7$),[11–16] have been developed for SIB anodes. However, the Na specific capacity of these materials is limited to 200 mA h g^{-1}. With a high surface area and structural flexibility, a two-dimensional (2D) material, graphene, is expected to be advantageous for use in SIB anodes. Although theoretical studies imply that the binding between Na and pristine graphene is too weak for Na storage compared with the cohesive energy of bulk Na, Datta *et al.* reveal that the introduction of defects in graphene could enhance the binding between Na and graphene and predict an enormous capacity (1450 mA h g^{-1}) in case of high defect concentration.[17] Another theoretical work indicates that heteroatoms B when doped into graphene could boost the Na storage capacity to 762 mA h g^{-1}.[18] David *et al.* have experimentally fabricated the reduced graphene oxide (rGO) paper electrode, which exhibits the maximum sodium charge capacity of ∼140 mA h g^{-1} at 100 mA g^{-1}.[19] Another monolayer structure MoS_2, is investigated as a potential candidate for the SIB anode and the Na specific capacity is predicted to reach as high as 335 mA h g^{-1}, which is larger than that of bulk MoS_2.[20,21] A Self-standing flexible electrode composed of few-layer MoS_2 and rGO flakes is prepared and shows a stable charge capacity of ∼230 mA h g^{-1} with good Na cycling ability.[22] However, the inferior carrier mobility of the monolayer MoS_2 limits its further application in the SIB anode.

Elemental phosphorus (P) can form Na_3P compounds with a theoretical capacity of around 2600 mA h g^{-1} (ref. 23) and has attracted a lot of attention from the scientific community. Kim *et al.* have fabricated the red phosphorus–carbon composite which exhibits an exceptionally high Na storage capacity of about 1800 mA h g^{-1}.[24–27] However, the overall performance of these materials is still unsatisfactory mainly due to the low rate capacity which may be attributed to the low electronic conductivity and large volumetric expansion of red phosphorus. Recently, phosphorene, 2D monolayer black phosphorus, has been successfully prepared using the mechanical exfoliation

[a] *State Key Laboratory of Digital Manufacturing Equipment and Technology and School of Mechanical Science and Engineering, Huazhong University of Science and Technology, Wuhan 430074, Hubei, People's Republic of China. E-mail: rongchen@mail.hust.edu.cn*

[b] *State Key Laboratory of Materials Processing and Die and Mould Technology and School of Materials Science and Engineering, Huazhong University of Science and Technology, Wuhan 430074, Hubei, People's Republic of China. E-mail: ywwen@mail.hust.edu.cn*

[c] *Department of Materials Science and Engineering, The University of Texas at Dallas, Richardson, Texas 75080, USA*

† Electronic supplementary information (ESI) available: Configurations of Na doped phosphorene at different Na concentrations and the structural stability studies of pristine phosphorene and $Na_{18}P_{48}$. See DOI: 10.1039/c5cp02419f

method and exhibits promising electronic properties and high carrier mobility,[28–30] which has been studied intensively for its potential application in electronics, optoelectronics, solar cells, photocatalysts and so on.[31–35] Kulish *et al.* have investigated the adsorption of a series of metal atoms (Li, Na, K, Cu *etc.*) on phosphorene. They reported that the binding energy of alkali metal atoms to phosphorene is stronger than the cohesive energy of the bulk structure, which implies the application of phosphorene in the storage of Li and Na.[36] A further theoretical study explores the Li doping properties on phosphorene[37] and predicts that the Li capacity on monolayer phosphorene can reach 432 mA h g^{-1}, which is higher than that of commercial graphite materials. However, the Li diffusion barrier on phosphorene is as high as 0.76 eV, which may cause an inferior rate capacity when phosphorene is used as a LIB anode. Since it has been reported that Na ions diffuse faster than Li ions in the layered structures,[38,39] phosphorene is expected to be more suitable to be used as the SIB anode. To date, the doping properties of Na in phosphorene are still not clear and the evaluation of phosphorene as the SIB anode should be of great interest.

In this work, we have systemically studied the structural, electronic, electrochemical as well as the diffusion properties of Na doped phosphorene based on first-principles calculations. Our results show that the phosphorene is able to accommodate the Na atoms. The calculated band structures and density of states (DOS) suggest that the adsorption of Na can enhance the electronic conductivity of phosphorene. Na atoms adsorbed on one side and both sides of phosphorene are systematically studied. It is found that the Na–Na interaction closely relates to the distance between Na atoms. A critical distance of about 4.35 Å for a strong Na–Na repulsion is identified and the Na specific capacity can be estimated to be 324 mA h g^{-1} for a close packing of Na on the surface of phosphorene. The Na^+/Na discharge curve related to the Na concentrations on phosphorene is simulated and several low and mild voltage plateaus are observed, which means that a steady and high work voltage can be achieved when phosphorene is used as a SIB anode. The diffusion barriers of Na atoms on phosphorene in both low and high Na concentrations are reported to be 40–63 meV, which implies that they may possess an outstanding rate capacity during the charge/discharge process. Our calculations provide a comprehensive understanding of the interaction between Na and phosphorene.

2. Computational models and methods

All calculations are performed within a density functional theory (DFT)[40,41] framework by using the projector-augmented-wave (PAW)[42] method, as implemented in the Vienna *ab initio* simulation package (VASP).[43–45] The exchange and correlation energy was treated *via* generalized gradient approximation (GGA) in the Perdew–Burke–Ernzerhof (PBE)[46] form. An energy cutoff of 400 eV is employed on the plane wave basis. The geometry optimization is performed till the Hellmann–Feynman force on each atom is smaller than 0.05 eV $Å^{-1}$. We adopt a 3 × 4 phosphorene supercell area of 13.89 Å × 13.20 Å with a vacuum thickness of 15 Å to avoid the interaction between image slabs. The numerical integration in the first Brillouin zone is performed using a Monkhorst–Pack[47] grid of 5 × 5 × 1. To check the convergence, we have compared the total energy to the ones calculated with finer *k*-mesh and found that the difference of total energy is smaller than 1 meV. A climbing image nudged elastic band (CI-NEB)[48] calculation is used to map the minimum energy path (MEP) of Na migration on phosphorene and to find the saddle points between two local minima for the system. Eight intermediate images are used for all CI-NEB calculations, which can map the MEP with reasonable accuracy.

3. Results and discussion

As shown in Fig. 1(a), different from pristine graphene, phosphorene is puckered with four P atoms in a unit cell (the red dashed framework). The optimized lattice constants are 4.63 Å along the *x* axis and 3.30 Å along the *y* axis, which are in good agreement with previous studies.[49,50] The calculated P–P distances and ∠P–P–P angles in (P_A–P_B, ∠$P_EP_AP_B$) and out (P_B–P_C, ∠$P_BP_CP_D$) of the plane are 2.22 Å, 96.0° and 2.26 Å, 104.2°, respectively. Moreover, the first Brillouin zone and symmetric *k* points of the phosphorene supercell have also been shown in Fig. 1(a). According to the symmetry of phosphorene, there are four inequivalent sites for Na doping in the unit cell on one side of phosphorene, which are labelled as T (on top of a P atom), B (on top of a P–P bond), Br (above the bridge site of two neighboring unbonded P atoms), and H (above the hollow site of the triangular neighboring unbonded P atoms) in Fig. 1(a). Table 1 summarizes the calculated binding energies (E_b), the optimized bond lengths between Na and the nearest P (d_{Na-P}) and the charge transfer of the adsorbed Na atom (ΔQ). E_b is defined as:

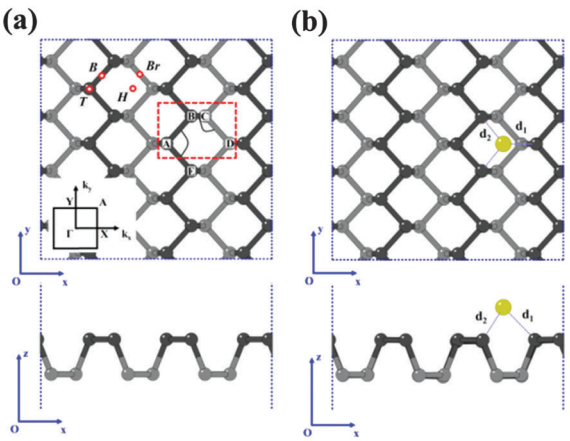

Fig. 1 Top-view and side-view of (a) possible doping sites on pristine phosphorene, (b) single Na atom adsorbed on the H-site of phosphorene. The phosphorus atoms in upper and bottom layers are highlighted by dark and light gray, respectively. The red dash square denotes the unit cell of phosphorene.

Table 1 Calculated binding energies (E_b), distances between Na and the nearest P of the optimized structures (d_{Na-P}) and the charge transfer of adsorbed Na atoms (ΔQ)

	B	Br	H	T
E_b (eV)	0.07	−0.24	−0.28	0.11
d_{Na-P} (Å)	2.85	2.80	2.83	2.73
ΔQ ($\|e\|$)	0.81	0.83	0.83	0.80

$$E_b = E_{phosphorene+Na} - E_{phosphorene} - nE_{Na,bcc} \quad (1)$$

where, $E_{phosphorene+Na}$, $E_{phosphorene}$ and $E_{Na,bcc}$ are the total energies of Na-adsorbed phosphorene, pristine phosphorene and a single Na atom in the bulk structure (bcc), respectively. Therefore, the more negative value of E_b means the stronger adsorption of Na on phosphorene as compared with the bulk structure. Note that the d_{Na-P} in all cases is about 2.80 Å, similar to the previous reported distance of Na adsorbed on graphene and MoS_2.[20,51] Among the four adsorption sites, the H site is the most favorable for Na with an E_b of −0.28 eV and the optimized structure of Na adsorbed onto the H site is shown in Fig. 1(b) (The other three adsorption configurations are shown in Fig. S1 in the ESI.†) The distances between the adsorbed Na atom and the nearest P atoms are 2.83 Å (d_1) and 2.92 Å (d_2), respectively. The negative binding energies of Na onto the H and Br sites reveal that Na atoms prefer to reside on the surface of phosphorene instead of clustering, suggesting that the phosphorene would be superior than graphene when used as a SIB anode.[17,18] The charge transfer between the Na atom and the phosphorene, ΔQ, is described by the Bader charge analysis.[52] The results in Table 1 show that the Na atoms adsorbed on H and Br sites involve the larger charge transfer to phosphorene, which would be responsible for the stronger binding energy.

Since the 2D monolayer phosphorene exhibits two sides of surfaces, we further explore the Na–Na interaction in the cases of one-side and both-side adsorptions on phosphorene. Fig. 2(a)–(d) illustrate the two Na atoms adsorbed on the same side, while (e)–(h) depict the two Na atoms adsorbed on the opposite sides individually. In each case, we have calculated E_b with different Na–Na distances. The optimized configurations (d_{Na-Na}), average binding energies ($\langle E_b \rangle$) as well as average charge transfer ($\langle \Delta Q \rangle$) per adsorbed Na atom are summarized in Fig. 2 and Table 2. To get a clear view of the binding energy and charge transfer to the Na–Na distance, they are plotted in Fig. 3(a) with the left and right parts denoting two Na atoms adsorbed on one-side and both-sides of phosphorene. We notice that the overall average binding energy per Na atom is slightly weaker than that of the single adsorbed Na atom (red dashed line) due to the Na–Na repulsion. In addition, $\langle E_b \rangle$ for both-side adsorption is stronger than that of one-side due to the weaker repulsion between the Na atoms in a larger distance. The important feature of Fig. 3(a) is that $\langle E_b \rangle$ of one-side adsorption increases sharply when d_{Na-Na} is shorter than 4.35 Å, which indicates that the repulsion between neighboring Na atoms becomes drastically strong within the critical distance.

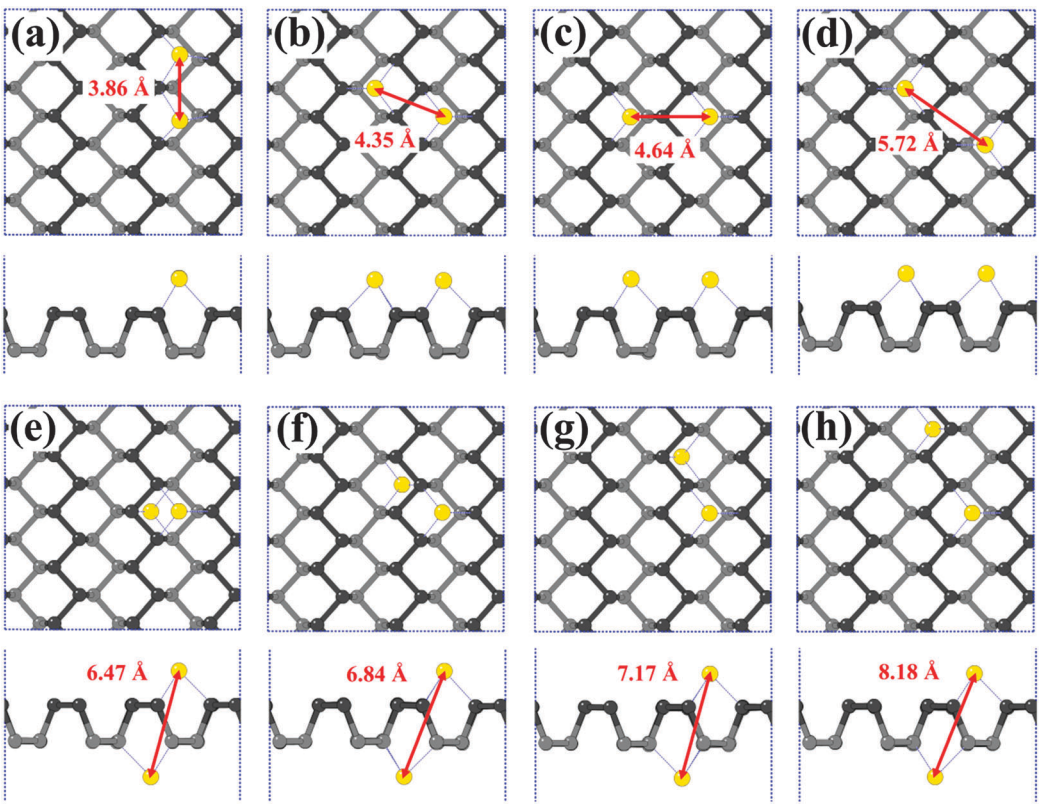

Fig. 2 Top-view and side-view of two Na atoms adsorbed on (a)–(d) one side and (e)–(h) both sides of phosphorene with different neighboring Na–Na distances.

Table 2 Calculated distances between Na atoms of the optimized structures (d_{Na-Na}), average binding energies ($\langle E_b \rangle$), and average charge transfer ($\langle \Delta Q \rangle$) of adsorbed Na atoms

	d_{Na-Na} (Å)	$\langle E_b \rangle$ (eV)	$\langle \Delta Q \rangle$ ($\langle e \rangle$)
One-side adsorption	3.86	−0.15	0.74
	4.35	−0.22	0.78
	4.64	−0.23	0.79
	5.72	−0.23	0.81
Both-sides adsorption	6.74	−0.29	0.80
	6.84	−0.28	0.80
	7.17	−0.26	0.81
	8.18	−0.25	0.82

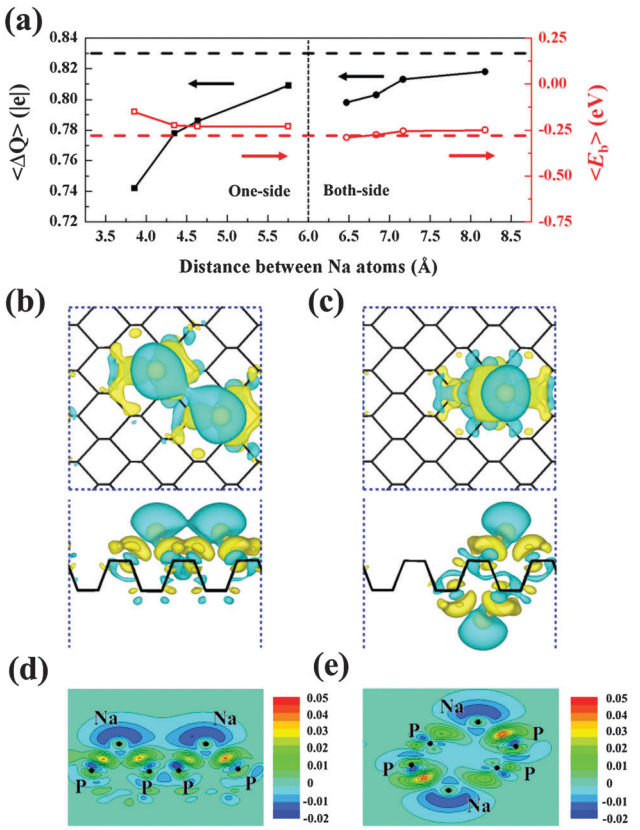

Fig. 3 (a) Average binding energies ($\langle E_b \rangle$) and charge transfer ($\langle \Delta Q \rangle$) of two Na atoms adsorbed on phosphorene as a function of the Na–Na distance. The black and red dash lines represent ΔQ and E_b of one Na adsorbed on phosphorene, respectively. (b) and (c) are the top and side views of the isosurface of the differential charge density of the structures shown in Fig. 2(d) and (e) with the increment level of $0.001a_0^{-3}$, where a_0 is the Bohr radius. The yellow and the grey-blue represent the positive and negative charges, respectively. (d) and (e) are corresponding contours of the differential charge density in side-views.

It is interesting that the average charge transfer between Na and phosphorene follows a reverse trend with the binding energy, which is reasonable since the binding strength is mainly determined by the electronic interaction between them. It seems to be an exception for the both-side adsorption that the shorter Na–Na distance (6.4 Å) yields a lower binding energy, which is probably attributed to the screening effect of the phosphorene towards the Na–Na repulsion.

Fig. 3(b) and (c) show the isosurface of differential charge density ($\Delta\rho$) of two Na atoms on phosphorene with one-side (Fig. 2(d)) and both-side (Fig. 2(e)) adsorption, respectively. $\Delta\rho$ is defined as:

$$\Delta\rho = \rho_{\text{phosphorene+2Na}} - \rho_{\text{phosphorene}} - \rho_{\text{Na-Na}} \quad (2)$$

where $\rho_{\text{phosphorene+2Na}}$, $\rho_{\text{phosphorene}}$ and $\rho_{\text{Na-Na}}$ are the charge densities of phosphorene with two adsorbed Na atoms, pristine phosphorene and an isolated Na dimer, respectively. There is obvious charge aggregation near the three nearest P atoms and charge dissipation around the Na–Na dimer, which indicates the formation of ion bonds between Na and phosphorene. The contours of $\Delta\rho$ for the two cases are shown from side-views in Fig. 3(d) and (e) to clarify this point. Since most of the charges of Na atoms are transferred to phosphorene, there should be a repulsive interaction between the two Na ions in such a short distance. For the both-side adsorption, the negative charged phosphorene locates between the two Na ions and thus has a more effective screening effect compared to the case of the one-side adsorption, where no screening medium exists between the two Na ions.

The band structure and density of states (DOS) have been calculated to investigate the electronic properties of phosphorene *via* Na intercalation. The band structure and DOS of the pristine phosphorene are shown in Fig. 4(a) and it exhibits a semiconducting behavior with the direct band gap of 0.94 eV, which agrees with the results of a previous study.[29] Upon one Na atom doping, the change of the band structure follows a rigid band picture and the Fermi level upshifts to cross the conductive band of phosphorene in Fig. 4(b), which implies a metallic behavior of the doped phosphorene. The partial

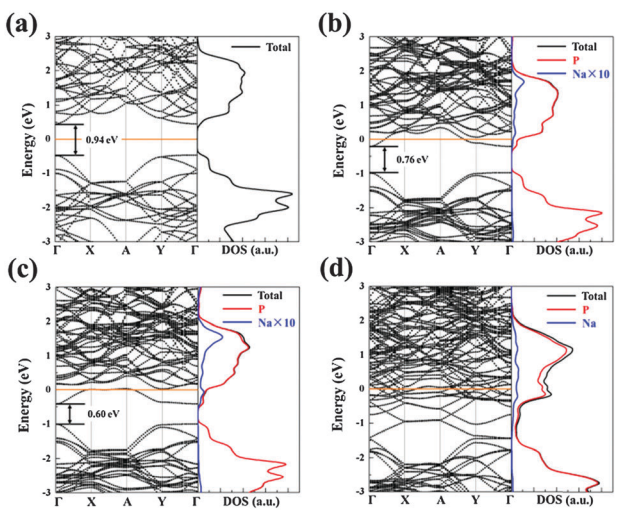

Fig. 4 Band structure and DOS of (a) pristine, (b) one Na adsorbed, (c) two Na with both sides adsorbed and (d) 18 Na atoms adsorbed phosphorene. The total DOS, partial DOS (PDOS) of P and Na atoms are plotted with black, red and blue lines, respectively. Note that the PDOS of Na atoms in (b) and (c) have been scaled up ten times.

density of state (PDOS) of Na atoms shows that the 2s electron of Na contributes to the DOS near the Fermi level. The injection of 2s electron from the Na atom into the conduction bands of phosphorene pushes the Fermi level upward, which corresponds to the charge transfer as mentioned above. Fig. 4(c) shows the band structure and DOS of two Na atoms doped phosphorene with both-side adsorption. The change is similar to that of one Na atom adsorption. Additionally, the energy gap between the original conduction band minimum and the valence band maximum of phosphorene decreases upon Na atom doping, which may be attributed to the enhanced orbital hybridization between Na 2s and P 2p. Our band structure and DOS calculations indicate that the Na doping can promote the electronic conductivity of the phosphorene.

Since there are many equivalent H sites on the both-side surface, it is expected that the phosphorene may exhibit high Na storage capacity. Knowing the critical distance for the Na–Na strong repulsion is about 4.35 Å as discussed above, one can roughly estimate the upper limit of Na capacity. In order to avoid the strong interaction between Na atoms, each Na atom should exclusively occupy an area of 4.35 Å × 4.35 Å, which contains 4.95 P atoms. Thus the maximum Na concentration with both-side adsorption could reach $Na_2P_{4.95}$, corresponding to a theoretical capacity of 350 mA h g^{-1} since the capacity (C) can be calculated by:

$$C = \frac{\lambda F}{M_P} \quad (3)$$

where λ is the atomic ratio of Na and P atoms, F is the Faraday constant (26.8 A h mol^{-1}), and M_P is the atomic mass of P (31 g mol^{-1}). On the other hand, we calculate the binding energies of the Na doped phosphorene at different concentrations ranging from Na_1P_{48} to $Na_{24}P_{48}$. For each concentration, several configurations (Fig. S2–S10 in the ESI†) are considered to yield the most stable one. Fig. 5 shows all calculated binding energies and the hull line (the black solid line). The hull curve is a convex polyline within the whole range of the coverage, with its vertices corresponding to all the true ground configurations of Na_xP_{48}. The total binding energy initially decreases with the increasing Na concentration and eventually saturates. Further Na intercalation would cause the weakening of the binding energy due to the strong Na–Na repulsion. One should note that even with the highest Na stoichiometry $Na_{24}P_{48}$, in which all H sites are occupied by Na atoms on both sides of phosphorene (Fig. S10 in the ESI†), the binding energy still is negative. However, its binding energy is about 0.41 eV less stable than the lowest point with a formula of $Na_{18}P_{48}$ as shown in Fig. 5(a) and the corresponding most stable configuration is shown in Fig. 5(b). Thus the largest Na concentration corresponds to a capacity of 324 mA h g^{-1}, which agrees well with our above estimation. We further plot the band structure and DOS of $Na_{18}P_{48}$ in Fig. 4(d) and find that the multiple Na atoms doping would increase the DOS of phosphorene near the Fermi level. The structural stability of the $p(2 \times 2)$ supercell of $Na_{18}P_{48}$ has also been considered during the charge/discharge processes by *ab initio* molecule dynamics simulation and the results show

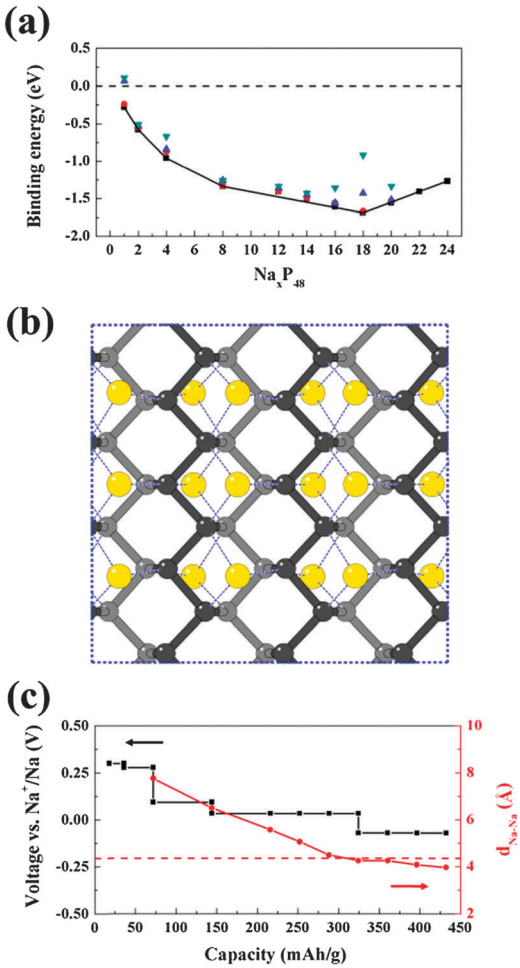

Fig. 5 (a) Colorful symbols give the calculated Na binding energies of different configurations and constructed black line of the convex hull indicates the ground states of phosphorene with different Na concentrations. (b) The most stable configurations of Na-doped phosphorene with the formula of $Na_{18}P_{48}$. (c) Corresponding voltage profile and the average distance between neighboring Na atoms as a function of Na uptake. The red dashed line represents the estimated critical distance of the Na–Na strong repulsion.

that the whole structure of phosphorene could be well-retained except for few atoms undergoing the conversion-type reaction in some local region (Fig. S12 in the ESI†). Moreover, the simulated results of fully discharged phosphorene with Na atoms removed can self-repair and recover well to the initial structure (Fig. S13 in the ESI†).

The electrochemical properties of the phosphorene as a SIB anode are investigated using Faraday's laws. The discharge process can be described as eqn (4), in which Δx indicates the number of intercalated Na atoms in each step:

$$Na_xP_{48} + \Delta xNa \rightarrow Na_{x+\Delta x}P_{48} \quad (4)$$

The voltage given by Faraday laws is:

$$V(x) = \frac{-\Delta G}{e\Delta x} \quad (5)$$

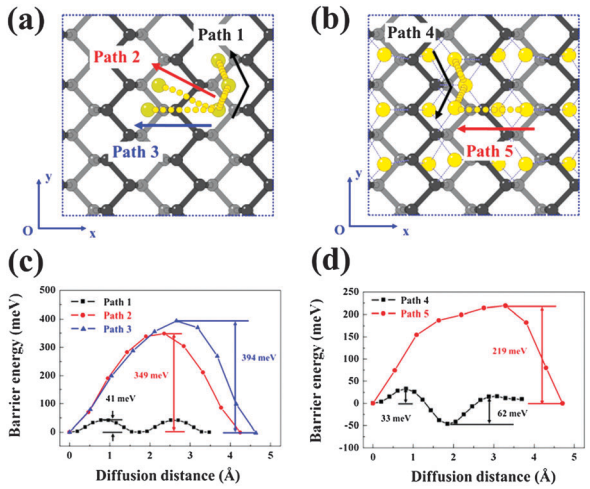

Fig. 6 (a) and (c) are the possible diffusion paths and calculated minimum energy paths of Na on the surface of phosphorene for low Na concentrations, (b) and (d) are diffusion paths and minimum energy paths for high Na concentrations.

where ΔG is the change of Gibbs free energy, which consists of three parts: $\Delta G = \Delta E + P\Delta V - T\Delta S$. In a solid-state reaction, $P\Delta V$ is on the order of 10^{-5} eV and $T\Delta S$ is on the order of the thermal energy ($\sim$0.026 eV). Thus ΔG can be well-approximated by the change of total energies (ΔE) obtained directly from first-principles calculations.[53] As shown in Fig. 5(c), there are two visible voltage plateaus during the discharge process. The first plateau is short with the Na^+/Na potential about 0.3 eV. The second one exhibits a relatively low and wide range plateau, which implies a high and stable working voltage when used as a SIB anode. The red curve in Fig. 5(c) represents the average distances between neighboring Na atoms at different Na concentrations. According to the most thermodynamically stable structure of compound $Na_{18}P_{48}$, the critical distance for the strong Na–Na repulsion should be about 4.3 Å and is in good agreement with the result of two Na atom adsorption.

Na-ion diffusion is an important factor affecting the rate capability of the SIBs. We focus on Na-ion diffusion on one-side of the phosphorene plane. Fig. 6(a) shows three possible diffusion paths for Na according to the structural symmetry. Path 1 illustrates the migration of Na along the zigzag channel in the *y* direction. In path 2, Na-ion will cross over a protruding P–P bond to the neighboring channel normally along the *y*-axis. Path 3 indicates the migration of Na-ion over a protruding P atom to the neighboring channel aside path 2. The corresponding MEPs of Na diffusion in these three paths are shown in Fig. 6(c). Clearly, path 1 has the lowest energy barrier of 41 meV, which is only 1/8 and 1/10 that of path 2 and path 3. This indicates that Na ions mainly diffuse along the *y* direction. When the Na ion migrates between different channels, it would preferentially adopt path 2 by climbing over a P–P bond instead of a P atom since the latter exhibits a 50 meV higher energy barrier. The Na diffusion in high concentrations has also been considered. We have chosen the highest doping concentration of $Na_{18}P_{48}$ as an example and employed the model of $Na_{17}P_{48}$ where a Na vacancy is created to investigate the migration of neighboring Na atoms. Two paths of Na diffusion, along and across the channel, are depicted as path 4 and path 5 in Fig. 6(b). The corresponding MEPs are calculated by CI-NEB and are plotted in Fig. 6(d). The energy barriers for the two paths, 33 meV and 62 meV, respectively, are also extremely low. It is interesting that the energy barrier of Na diffusion along path 5 is about half of that in path 1 when the Na atom migrates to another channel, which indicates that the Na–Na repulsion benefits the Na diffusion in closely aligned patterns. We note that the Na diffusion barriers in both low and high concentrations are less than 70 meV, which is much lower than that of Li on phosphorene and Na on other reported 2D materials.[18,20,37,54]

4. Conclusions

Based on first-principles calculations, we have systemically studied the adsorption and diffusion behaviors of Na on phosphorene. Our results indicate that phosphorene is able to accommodate the storage of Na. Upon the investigation of the Na–Na interaction on phosphorene, a critical Na–Na repulsion distance has been found and the Na intercalation capacity can be estimated to be 324 mA h g^{-1}. The calculated discharge curve of Na^+/Na reveals that phosphorene exhibits a stable voltage profile within a wide range. The diffusion energy barrier of Na on phosphorene is extremely low ($\sim$40 meV), which implies that the phosphorene may exhibit outstanding rate capacity when used as a SIB anode.

Acknowledgements

This work is supported by the National Basic Research Program of China (2013CB934800), the National Natural Science Foundation of China (Grant 51302094 and 51101064), and the Hubei Province Funds for Distinguished Young Scientists (2014CFA018 and 2015CFA034). Rong Chen acknowledges the Thousand Young Talents Plan the Recruitment Program of Global Experts and Changjiang Scholars and Innovative Research Team in University (No.: IRT13017). The calculations have been performed at the Texas Advanced Computing Center (TACC) at The University of Texas at Austin (http://www.tacc.utexas.edu).

Notes and references

1 J. M. Tarascon and M. Armand, *Nature*, 2001, **414**, 359–367.
2 Y. W. Wen, X. Liu, X. B. Duan, K. Cho, R. Chen and B. Shan, *J. Phys. Chem. C*, 2013, **117**, 4951–4956.
3 M. Dahbi, N. Yabuuchi, K. Kubota, K. Tokiwa and S. Komaba, *Phys. Chem. Chem. Phys.*, 2014, **16**, 15007–15028.
4 J. Sun, G. Y. Zheng, H. W. Lee, N. Liu, H. T. Wang, H. B. Yao, W. S. Yang and Y. Cui, *Nano Lett.*, 2014, **14**, 4573–4580.
5 M. D. Slater, D. Kim, E. Lee and C. S. Johnson, *Adv. Funct. Mater.*, 2013, **23**, 947–958.

6 S. W. Kim, D. H. Seo, X. H. Ma, G. Ceder and K. Kang, *Adv. Energy Mater.*, 2012, **2**, 710–721.
7 X. F. Yu, G. Giorgi, H. Ushiyama and K. Yamashita, *Chem. Phys. Lett.*, 2014, **612**, 129–133.
8 D. P. DiVincenzo and E. J. Mele, *Phys. Rev. B: Condens. Matter Mater. Phys.*, 1985, **32**, 2538–2553.
9 D. A. Stevens and J. R. Dahn, *J. Electrochem. Soc.*, 2001, **148**, A803–A811.
10 S. Y. Hong, Y. Kim, Y. Park, A. Choi, N. Choi and K. T. Lee, *Energy Environ. Sci.*, 2013, **6**, 2067–2081.
11 R. Alcantara, J. M. Jimenez-Mateos, P. Lavela and J. L. Tirado, *Electrochem. Commun.*, 2001, **3**, 639–642.
12 K. L. Hong, L. Qie, R. Zeng, Z. Q. Yi, W. Zhang, D. Wang, W. Yin, C. Wu, Q. J. Fan, W. X. Zhang and Y. H. Huang, *J. Mater. Chem. A*, 2014, **2**, 12733–12738.
13 H. Xiong, M. D. Slater, M. Balasubramanian, C. S. Johnson and T. Rajh, *J. Phys. Chem. Lett.*, 2011, **2**, 2560–2565.
14 K. Y. Chen, W. X. Zhang, Y. Liu, H. P. Zhu, J. Duan, X. H. Xiang, L. H. Xue and Y. H. Huang, *Chem. Commun.*, 2015, **51**, 1608–1611.
15 J. Xu, C. Z. Ma, M. Balasubramanian and Y. S. Meng, *Chem. Commun.*, 2014, **50**, 12564–12567.
16 C. Deng, S. Zhang, Z. Dong and Y. Shang, *Nano Energy*, 2014, **4**, 81–87.
17 D. Datta, J. W. Li and V. B. Shenoy, *ACS Appl. Mater. Interfaces*, 2014, **6**, 1788–1795.
18 C. Ling and F. Mizuno, *Phys. Chem. Chem. Phys.*, 2014, **16**, 10419–10424.
19 L. David and G. Singh, *J. Phys. Chem. C*, 2014, **118**, 28401–28408.
20 J. C. Su, Y. Pei, Z. H. Yang and X. Y. Wang, *RSC Adv.*, 2014, **4**, 43183–43188.
21 M. Mortazavi, C. Wang, J. K. Deng, V. B. Shenoy and N. V. Medhekar, *J. Power Sources*, 2014, **268**, 279–286.
22 L. David, R. Bhandavat and G. Singh, *ACS Nano*, 2014, **8**, 1759–1770.
23 N. Yabuuchi, Y. Matsuura, T. Ishikawa, S. Kuze, J. Y. Son, Y. T. Cui, H. Oji and S. Komaba, *ChemElectroChem*, 2014, **1**, 580–589.
24 Y. J. Kim, Y. W. Park, A. Choi, N. S. Choi, J. Kim, J. Lee, J. H. Ryu, S. M. Oh and K. T. Lee, *Adv. Mater.*, 2013, **25**, 3045–3049.
25 J. F. Qian, X. Y. Wu, Y. L. Cao, X. P. Ai and H. X. Yang, *Angew. Chem., Int. Ed.*, 2013, **52**, 4633–4636.
26 W. J. Li, S. L. Chou, J. Z. Wang, H. K. Liu and S. X. Dou, *Nano Lett.*, 2013, **13**, 5480–5484.
27 J. X. Song, H. X. Yu, M. L. Gordin, S. Hu, R. Yi, D. H. Tang, T. Walter, M. Regula, D. W. Choi, X. L. Li, A. Manivannan and D. H. Wang, *Nano Lett.*, 2014, **14**, 6329–6335.
28 L. Li, Y. Yu, G. J. Ye, Q. Ge, X. Ou, H. Wu, D. Feng, X. H. Chen and Y. Zhang, *Nat. Nanotechnol.*, 2014, **9**, 372–377.
29 H. Liu, A. T. Neal, Z. Zhu, Z. Luo, X. Xu, D. Tománek and P. D. Ye, *ACS Nano*, 2014, **8**, 4033–4041.
30 W. Lu, H. Nan, J. Hong, Y. Chen, C. Zhu, Z. Liang, X. Ma, Z. Ni, C. Jin and Z. Zhang, *Nano Res.*, 2014, **7**, 853–859.
31 J. S. Qiao, X. H. Kong, Z. X. Hu, F. Yang and W. Ji, *Nat. Commun.*, 2014, **5**, 4475.
32 V. Tran and L. Yang, *Phys. Rev. B: Condens. Matter Mater. Phys.*, 2014, **89**, 245407.
33 H. Y. Lv, W. J. Lu, D. F. Shao and Y. P. Sun, *Phys. Rev. B: Condens. Matter Mater. Phys.*, 2014, **90**, 085433.
34 J. Dai and X. C. Zeng, *J. Phys. Chem. Lett.*, 2014, **5**, 1289–1293.
35 B. S. Sa, Y. L. Li, J. S. Qi, R. Ahuja and Z. M. Sun, *J. Phys. Chem. C*, 2014, **118**, 26560–26568.
36 V. V. Kulish, O. I. Malyi, C. Perssoncd and P. Wu, *Phys. Chem. Chem. Phys.*, 2015, **17**, 992–1000.
37 S. J. Zhao, W. Kang and J. M. Xue, *J. Mater. Chem. A*, 2014, **2**, 19046–19052.
38 S. P. Ong, V. L. Chevrier, G. Hautier, A. Jain, C. Moore, S. Kim, X. H. Ma and G. Ceder, *Energy Environ. Sci.*, 2011, **4**, 3680–3688.
39 R. Tripathi, S. M. Wood, M. S. Islam and L. F. Nazar, *Energy Environ. Sci.*, 2013, **6**, 2257–2264.
40 P. Hohenberg and W. Kohn, *Phys. Rev.*, 1964, **136**, B864–B871.
41 W. Kohn and L. J. Sham, *Phys. Rev.*, 1965, **140**, A1133–A1138.
42 G. Kresse and D. Joubert, *Phys. Rev. B: Condens. Matter Mater. Phys.*, 1999, **59**, 1758–1775.
43 G. Kresse and J. Hafner, *Phys. Rev. B: Condens. Matter Mater. Phys.*, 1993, **47**, 558–561.
44 G. Kresse and J. Hafner, *Phys. Rev. B: Condens. Matter Mater. Phys.*, 1994, **49**, 14251–14269.
45 G. Kresse and J. Hafner, *Comput. Mater. Sci.*, 1996, **6**, 15–50.
46 J. P. Perdew, K. Burke and M. Ernzerhof, *Phys. Rev. Lett.*, 1996, **77**, 3865–3868.
47 H. J. Monkhorst and J. D. Pack, *Phys. Rev. B: Solid State*, 1976, **13**, 5188.
48 G. Henkelman and H. J. Jónsson, *J. Chem. Phys.*, 2000, **113**, 9978–9985.
49 Y. Li, S. X. Yang and J. B. Li, *J. Phys. Chem. C*, 2014, **118**, 23970–23976.
50 Z. Zhu and D. Tománek, *Phys. Rev. Lett.*, 2014, **112**, 176802.
51 Y. Wei and K. Manzhos, *MRS Commun.*, 2013, **3**, 171–175.
52 G. Henkelman, A. Arnaldsson and H. Jonsson, *Comput. Mater. Sci.*, 2006, **36**, 354–360.
53 M. K. Aydinol, A. F. Kohan and G. Ceder, *J. Power Sources*, 1997, **68**, 664–668.
54 V. V. Kulish, O. I. Malyi, M. F. Ng, Z. Chen, S. Manzhos and P. Wu, *Phys. Chem. Chem. Phys.*, 2014, **16**, 4260–4267.